ACS Partner Journal

CHEM & BIO ENGINEERING

pubs.acs.org/ChemBioEng

Article

Modulating the Coordination Environment of Cu Sites for Highly Selective CO_2 Electroreduction to Ethylene

Wenfu Luo, Shijie Li, Yao Shen,* Shihan Zhang, Wei Li, and Sujing Li*

Cite This: *Chem Bio Eng.* 2024, 1, 836−845

Read Online

ACCESS | Metrics & More | Article Recommendations | Supporting Information

ABSTRACT: Carbon dioxide (CO_2) can be reduced to a variety of value-added products by the electrochemical reduction of CO_2 (ERC). Modulating the coordination environment of the Cu sites can effectively optimize the selectivity and activity of the reduction process. In this work, we report a facile strategy to regulate the coordination environment of Cu sites for improving the Faradaic efficiency (FE) of ethylene. Room-temperature Ar plasma with different powers and treating times was employed to partially remove the 2,5-dihydroxyterephthalic moieties from the structure of Cu-MOF-74, thus resulting in more unsaturated coordinated Cu sites and lower oxidation state. The structure distortion and electron configuration change of Cu-MOF-74-P was observed from electron paramagnetic resonance (EPR). Meanwhile, the proportion of Cu^+ in Cu-MOF-74-P has increased significantly. By combination of XAFS and in situ DRIFTS, it was shown that the coordination number of Cu-MOF-74-P has decreased from 2.7 to 1.6, thus facilitating the formation of more *CO intermediates on the surface during the reduction process. This modification strategy successfully increased the Faradaic efficiency of C_2H_4 in the product up to 48%, which was 3.2 times of its original performance. This work provides some guidance for the design of catalysts with tailored selectivity during CO_2 electroreduction.

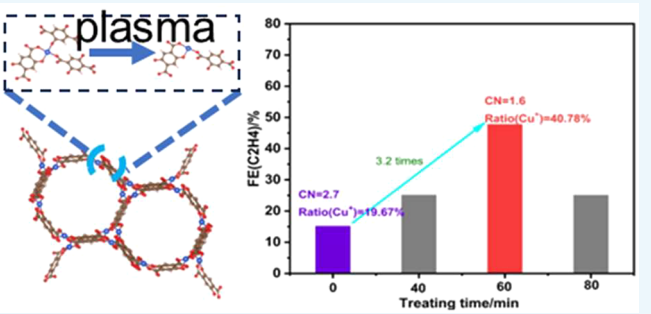

KEYWORDS: *CO_2 reduction, low Coordination number, selectivity, C_2H_4, plasma treatment, *CO coverage*

1. INTRODUCTION

The electrochemical reduction of CO_2 (ERC) into valuable chemicals and renewable fuels of high energy density powered by renewable electricity offers a cost-effective and environmental way toward the carbon neutrality.[1−3] CO_2 can be reduced to generate C_1 or C_2 or C_{2+} products including methane (CH_4), ethylene (C_2H_4), ethanol (C_2H_5OH), propanol (C_3H_7OH), etc., with different numbers of transferred protons and electrons.[4] With lots of effort, there has exhibited a very high selectivity of over 98.4% toward CO[5] and 92% to HCOOH[6] production. However, it is still challenging to improve the proportion of the C_2 and C_{2+} product in products up to date, for that such as the wide product distribution, high overpotentials, the reactor and the electrolyte could influence a lot about the C_2 selectivity.[7] Notably, C_2H_4 is a regarded CO_2 electroreduction C_2 product with a wide range of applications and high values of 1232.5−1300.6 $/t. Thus, to boost C_2H_4 production, we need to develop an optimal catalyst to improve its selectivity. Among all kinds of metal catalysts for ERC, Cu catalyst is very unique for moderate adsorption of intermediates and its ability to induce *CO dimerization to achieve high C_2H_4 conversion.[8] However, there are still many challenges such as low product selectivity and unsatisfactory FE[9,10] hampering the practical application of Cu-based catalysts.

There are plenty of strategies that can be used to improve the performance of electrochemical reduction of CO_2 (ERC), such as modulating the surface structure, regulating the active valence state, introducing the oxygen vacancies, changing the particle size and the pore size, and using tandem catalysts. Typically, the ECR's activity and selectivity are influenced a lot by the CO_2 activation and the adsorption strength of the intermediates (such as *CO and *H) on the active metal site.[11,12] Many studies showed that the performance of electrocatalysts is closely related to the coordination environment of catalytic sites.[13] Delicately tuning the coordination number and electronic structure of catalytic sites would enhance the adsorption of intermediates and ultimately influence the distribution of products.[14,15] Specifically, the low coordination number promotes a reduced oxidation state from +2 to +1 and higher local electronic densities of the metal center,[16,17] which is beneficial to adsorb and activate the CO_2 molecules and optimize the adsorption strength of inter-

Received: January 23, 2024
Revised: March 13, 2024
Accepted: April 2, 2024
Published: April 10, 2024

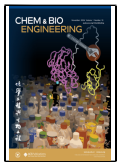

mediates. Theoretical studies[18,19] have shown that the unsaturated coordination structures allow CO_2 and intermediates adsorbed on metal atoms more stably, thus increasing the concentration of the reaction intermediates *CO. So it will promote the C−C coupling of the *CO and C_2 selectivity. Also, the +1-oxidation state Cu could help to reduce the energy barrier of the C−C coupling process. Therefore, abundant low coordination metal sites can significantly enhance the total reaction current and product selectivity. Furthermore, the low coordination environment creates a space around the metal sites, thus facilitating the bonding between the intermediates and the metal center. However, the intrinsic mechanism in modulating the coordination number of Cu atoms and how the coordination environment of Cu sites influences the electrocatalytic performance remain elusive.

Herein, we applied metal−organic framework (MOF) material, which is a crystalline porous material, to get an unsaturated Cu coordination structure to promote C_2H_4 generation. MOFs have attracted great attention due to their unique advantages such as large surface area, abundant pore structure, and ease of framework modification, thus making them highly promising in the catalytic field.[20] As for in ERC, MOFs have sufficient unsaturated single atom sites and thus have excellent performance in capturing and activating CO_2.[21,22] The adjustable porous framework structure provides a feasible way to achieve unsaturated metal sites, thereby improving the selectivity and activity.[23,24] Through high-temperature calcination, atom doping or chemical etching, the MOF can effectively promote the unsaturated coordination of Cu in the Cu-MOF.[25] However, these processes are either energy- or time-consuming. Compared to them, plasma treatment is a very convenient and energy-saving technology to modify the catalyst, which we could learn from the prior studies.[26,27] What is more, with noble gases plasma such as Ar plasma, it will not introduce other atoms into the structure.[28] Hence, the plasma strategy supplies a suitable way to engrave the coordination bonds to form unsaturated metal sites.

In this work, we used mild Ar plasma to bombard the Cu-based MOF-74 (Cu-MOF-74) to remove partial organic ligands at room temperature. This process maintains the spatial structure of the MOF and effectively modulates the coordination environment of Cu from 2.7 to 1.6, also regulating the active valence state of Cu to increase the ratio of unsaturated Cu^+ to 40.78%. X-ray absorption fine spectroscopy (XAFS) was also carried out to investigate the change of coordination number of the catalyst after the treatment. Meanwhile, in situ DRIFTS was employed to monitor the changes of the amount of *CO intermediates on the surface of the catalyst during the CO_2 reduction process. The unsaturated Cu sites and lower valence state obtained by plasma bombardment successfully increased the $FE_{C_2H_4}$ to 48%, which was 3.2 times that of the original in the flow cell. This work provides a convenient way to promote unsaturated coordination of MOF-based Cu catalysts to improve the C_2H_4 selectivity and activity of the ERC.

2. EXPERIMENTAL SECTION

2.1. Chemicals and Materials. The chemicals and solvents were purchased commercially and used without further purification. 2,5-Dihydroxyterephthalic acid (≥0.98) was obtained from Maya Reagent (Shanghai, China). Copper acetate ($Cu(CH_3COO)_2{\cdot}H_2O$, ≥0.99) was purchased from Sigma-Aldrich (Germany). Methanol (AR) was purchased from Sinopharm Chemical Reagent Co., Ltd. (Shanghai, China). The ultrapure water (Resistivity reaches 18.2 MΩ cm at 25 °C) was used throughout the experiment process with an ECO-S15 ultrapure water system. Anion exchange membrane (3PK-130) was purchased online.

2.2. Synthesis of Cu-MOF-74. Cu-MOF-74 ($C_8H_6Cu_2O_8$, Mr = 357) was synthesized by reacting copper acetate ($Cu(CH_3COO)_2{\cdot}H_2O$, AR) and 2,5-dihydroxyterephthalic acid (AR) based on the previous research.[29,30] Dissolve about 0.4 g of $Cu(CH_3COO)_2{\cdot}H_2O$ into 10 mL of CH_3OH with stirring to obtain a well-distributed solution of $Cu(CH_3COO)_2$ (10 ml, 40 g/L). Meanwhile, 0.2 g of DHTP (2,5-dihydroxyterephthalic acid) was added into 5 mL of CH_3OH under stirring for 20 min to be uniform. Then the above mixture was added dropwise to the $Cu(CH_3COO)_2$ solution. Keep stirring for 24 h at room temperature until the mixture changed into reddish brown. The Cu-MOF-74 crystalline solid was collected by centrifugation for 5 min at a speed of 8000 rpm. Soak the product in a certain amount of methanol overnight for 4 times to completely remove impurities. Finally, Cu-MOF-74 was collected by centrifugation again and dried in vacuum at 85 °C for 5 h.

2.3. Plasma Treatment of Cu-MOF-74. Cu-MOF-74 was ground to a size below 60 mesh prior to get a better plasma treatment. The Cu-MOF-74 powder was placed on the bottom of the porcelain boat, and it was put into the plasma enhanced chemical vapor deposition instrument (PECVD) in the quartz tube at an appropriate position. After the argon gas replacement for three times, the air in the pipeline was exhausted. Then the Ar flow rate was fixedly set at 20 mL/min, different powers and treating times were set while keeping the overall output energy constant to select the optimal treatment power. Preliminary experiments revealed that the catalyst was prone to denaturation and decomposition under a high-temperature plasma treatment. Thus, the plasma treatment was carried out at room temperature.

2.4. In Situ DRIFTS. In situ DRIFTS experiments were measured on a semicylindrical silicon crystal to monitor reaction intermediates. The silicon crystal was polished on both 300 and 50 nm Al_2O_3 polishing powders to obtain a smooth surface. The silicon crystals were then cleaned with water and ethanol under ultrasonication each for five times. Then it was treated with a mixture of H_2O_2 and concentrated sulfuric acid, which would attach a large number of hydroxyl radicals to the surface of the silicon crystals. Then the silicon crystals were etched in 40 wt % of NH_4F solution for about 90 s to prepare for the gilding process. The gold plating was then carried out in a gold plating solution in a thermostatic water bath at 54 °C. After that, the entire electrode reaction system was acid-washed in dilute sulfuric acid by CV polarization, and then, the water on the gold foil was blown dry with N_2. Catalyst ink was prepared by dispersing 1 mg of catalyst into 240 μL of water, 710 μL of isopropanol, and 50 μL of Nafion solution, and 40 μL of inks was dropped on the center of the gold foil and tested after drying under infrared light. After the background acquired by the infrared (IR) instrument stabilized, linear sweep voltammetry (LSV) was performed at 0 to −1.8 V vs Ag/AgCl, and the recording of intermediate IR information began at the same time.

2.5. CO_2 Electroreduction Analysis. The ERC activity evaluation experiments were carried out in a flow cell (Figure S9) by dispersing 10 mg of catalyst in 950 μL of isopropanol and 50 μL of Nafion solution and being mixed for half an hour under sonication, then 300 μL of ink was applied uniformly by dropwise addition to 1 cm × 3 cm size carbon paper to ensure that the density of catalyst was 1 mg/cm^2, and then the carbon paper was dried under infrared light for use.

The electrolyte is $KHCO_3$ of 0.5 mol/L by passing CO_2 gas into the K_2CO_3 solution for a sufficiently long time, which is also filled with CO_2. The cathode liquid peristaltic pump speed was set to 20 rpm, while the anode liquid speed was adjusted to the largest. The CO_2 gas flow rate was set to 10 mL/min. The constant potentials are generated using an electrochemical workstation, and the number of charges transferred by the reaction process can be easily obtained.

The gas products (including CO, CH_4, C_2H_4, H_2, etc.) were analyzed using a gas chromatograph with a thermal conductivity

https://doi.org/10.1021/cbe.4c00021
Chem Bio Eng. 2024, 1, 836−845

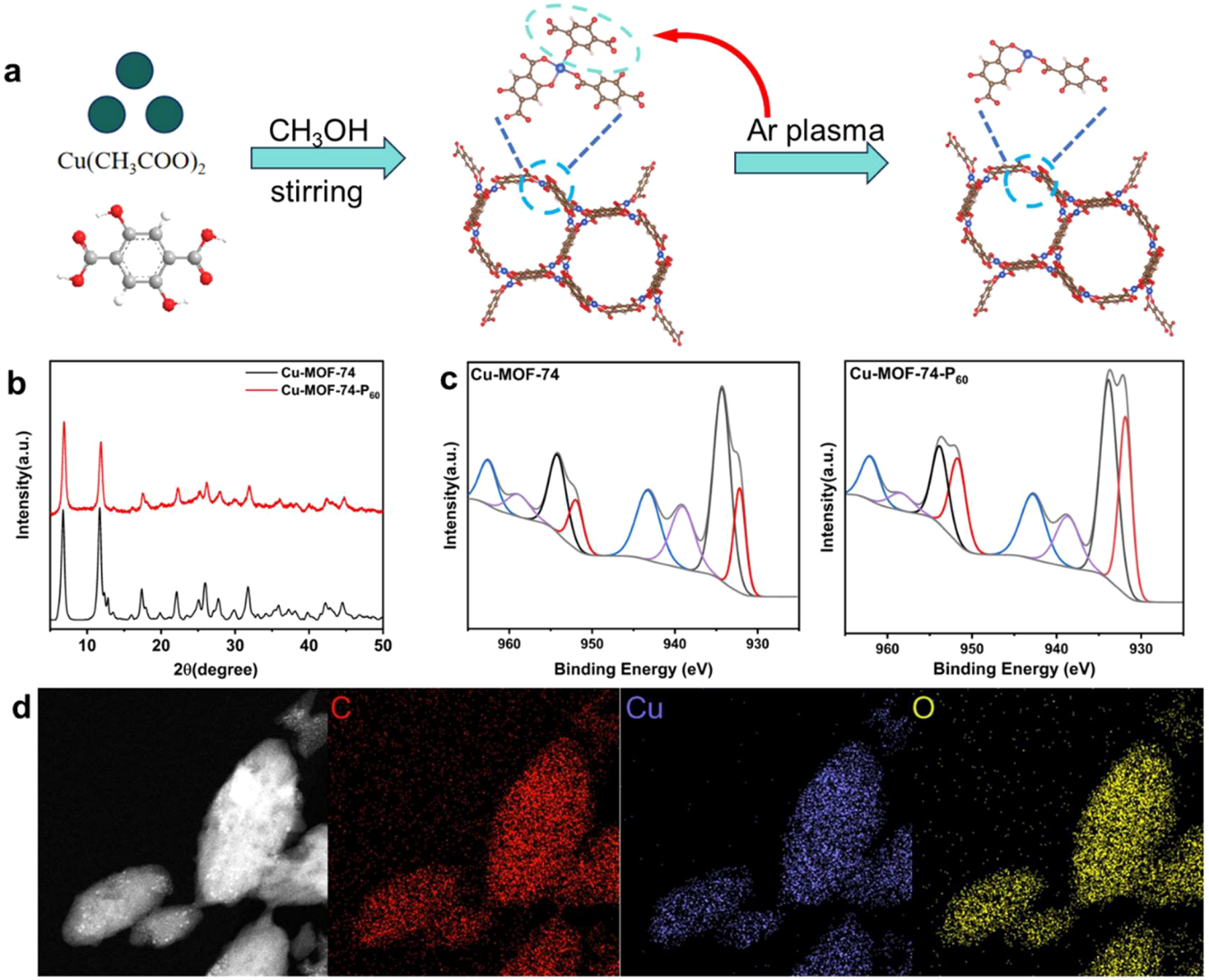

Figure 1. (a) Schematic for preparation of Cu-MOF-74 and Cu-MOF-74-P. (b) XRD pattern of as-prepared Cu-MOF-74 and 10 W 60 min plasma treated Cu-MOF-74 to analyze the phase composition. (c) XPS fine spectra of as-prepared Cu-MOF-74 and Cu-MOF-74-P_{60} with the BE from 925 to 965 eV. (d) 100 nm TEM image of as-prepared Cu-MOF-74, and TEM EDS image of different atoms of as-prepared Cu-MOF-74, different colors stand for different atoms, red for the C atom, purple for the Cu atom, and yellow for the O atom.

detector (TCD) and a flame ionization detector (FID), model GC-9790II. The liquid phase products (HCOOH, CH_3COOH, C_2H_5OH, etc.) were then subjected to NMR hydrogen spectroscopy with heavy water to shield the relevant signals and dimethyl sulfoxide as an internal standard substance.

2.6. XAFS Analysis. The whole XAFS analysis process was carried out at the BL11B beamline with a Si (111) crystal monochromator at the Shanghai Synchrotron Radiation Facility (SSRF) (Shanghai, China). Before the beamline analysis, the catalyst was shaped into a 1 cm diameter sheet and sealed with Kapton tape film. The XAFS data and spectra were recorded at room temperature with a four-channel silicon drift detector (SDD) Bruker 5040. Cu K-edge extended X-ray absorption fine structure (EXAFS) spectra were recorded in the transmission mode. Negligible changes in the line shape and peak position of the Cu K-edge X-ray absorption near edge structure (XANES) spectra were observed between the two scans performed on one same sample. The XAFS spectra of these standard samples (CuPC, CuO, Cu_2O, and Cu foil) were recorded in transmission mode. The spectra were processed and fitted by the software codes Demeter.

3. RESULTS AND DISCUSSION

3.1. Catalyst Preparation and Characterization. Cu-MOF-74 ($C_8H_6Cu_2O_8$) was prepared with cupric acetate and 2,5-dihydroxyterephthalic acid using methanol as solution at room temperature[29,30] (Figure 1a). As the X-ray diffraction (XRD) patterns shown in Figure 1b, the two main characteristic peaks at 6.5° and 11.5° were located at the same position reported by Zheng,[30] demonstrating the Cu-MOF-74 was successfully synthesized. Scanning electron microscopy (SEM) (Figure S1) and transmission electron microscopy (TEM) were also shown in Figure 1d, which exhibited a shape of conical crystals, with a group size of no more than 600 nm. From TEM energy dispersive X-ray spectroscopy (EDS) mapping (Figure 1d), we could see that the Cu, C, and O elements coexisted and distributed well among the skeleton.[31] Then, to modulate the coordination structure and the oxidation state of Cu in Cu-MOF-74, mild Ar plasma treatment had been applied on Cu-MOF-74 to partially engrave the organic ligands in the MOF (Figure 1a). As we could see, no obvious difference was shown on morphology of

https://doi.org/10.1021/cbe.4c00021
Chem Bio Eng. 2024, 1, 836−845

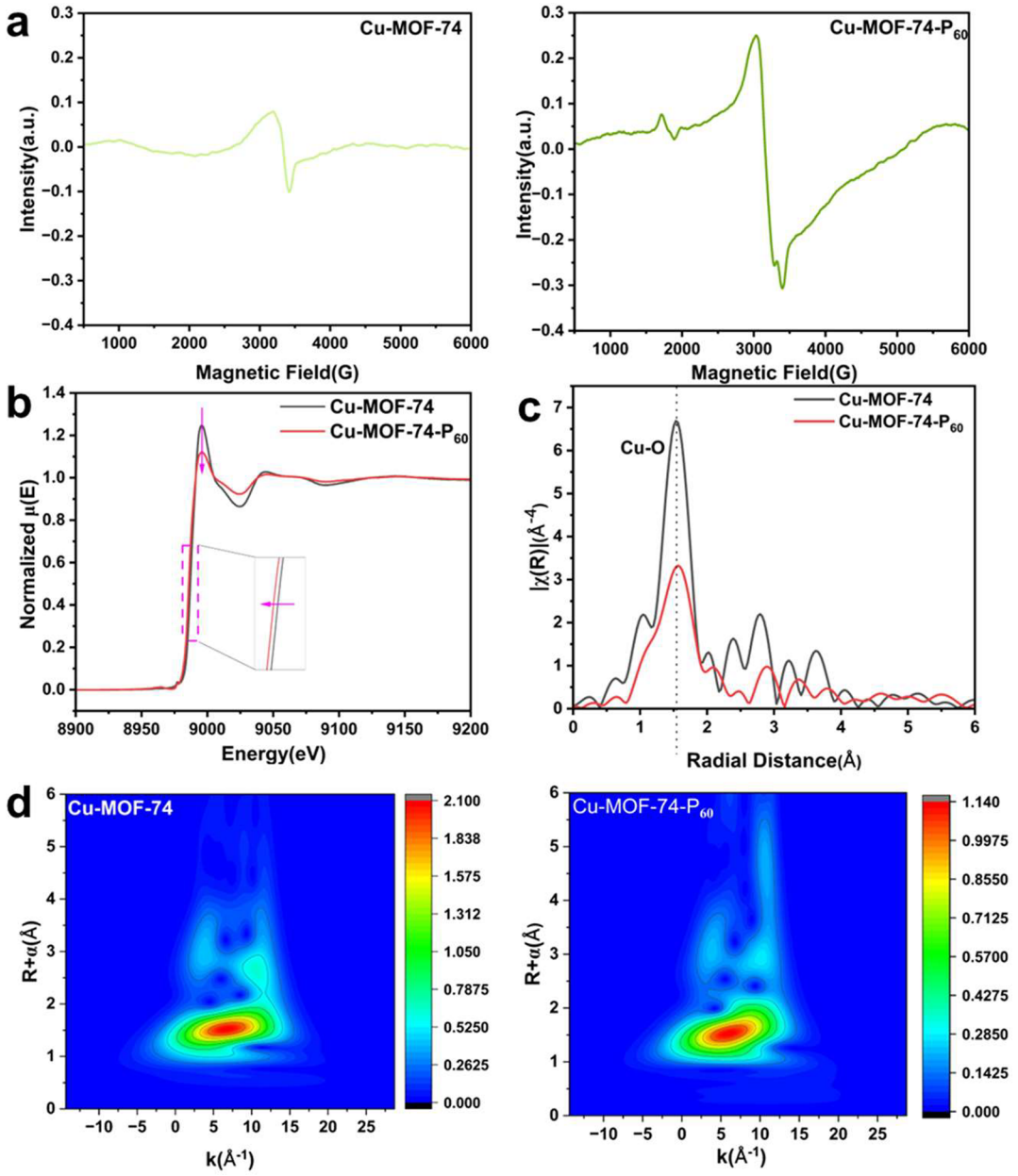

Figure 2. (a) EPR figure of Cu-MOF-74 and Cu-MOF-74-P_{60} to verify the structure distortion. (b) Normalized XANES spectra at the Cu K-edge of as-prepared Cu-MOF-74 and 10 W 60 min plasma treated Cu-MOF-74. (c) Fourier transformations of k^3-weighted EXAFS spectra of as-prepared Cu-MOF-74 and 10 W 60 min plasma treated Cu-MOF-74. (d) Wavelet transform spectrum from the χ(K).

the as-prepared Cu-MOF-74 and Cu-MOF-74-P_{60} (the MOF treated by 10 W Ar plasma for 60 min was named Cu-MOF-74-P_{60}) according to SEM and TEM (Figures S2 and S3). The EDS of the Cu-MOF-74-P_{60} also indicated that Cu, C, and O elements distributed well on the catalyst, and there were no Cu atoms gathered in clusters, demonstrating that the structure of Cu-MOF-74-P_{60} was not destroyed after plasma. Besides, from the XRD patterns in Figure 1b, similar peaks were exhibited for Cu-MOF-74 and Cu-MOF-74-P_{60}, with slight decrease of the intensity after the treatment, indicating the decrease of the crystallinity that might be attributed to the structure decomposition after the treatment.[32]

We then performed X-ray photoelectron spectroscopy (XPS) analysis on the samples before and after the treatment. From the XPS fine spectrum shown in Figure 1c, the feature peaks of Cu 2p spectrum for both Cu-MOF-74 and Cu-MOF-74-P_{60} catalysts were located at 931.86 and 951.67 eV, being attributed to the Cu $2p_{1/2}$ and Cu $2p_{3/2}$ of Cu^+ and Cu^0.[33] The other two relative peaks at 933.82 and 953.79 eV were from the Cu $2p_{1/2}$ and Cu $2p_{3/2}$ of Cu^{2+}. Similarly, the satellite peaks at 938.67, 942.78, 958.83, and 960.68 eV also attributed to Cu^{2+}. In the XPS fine spectrum, the intensity of the Cu^+ and Cu^0 peak of Cu-MOF-74-P_{60} increased significantly, compared with those of the as-prepared Cu-MOF-74 in Figure 1c. Cu auger electron spectroscopy (AES) was further carried out to distinguish the content of Cu^+ and Cu^0 from each other. As the result exhibited, the Cu LMM spectra (Figure S6) showed that there was only a Cu^+ feature peak locating at 570.2 eV. No clear Cu^0 peak at 567.9 eV was found in it, indicating that there was only Cu^+ and Cu^{2+} in the Cu-MOF-74. Compared to Cu-MOF-74, the key change in the fine spectrum for Cu-MOF-74-P_{60} was that satellite peaks got weaker and the feature peak for

https://doi.org/10.1021/cbe.4c00021
Chem Bio Eng. 2024, 1, 836−845

Cu^+ got stronger, suggesting that the valence state was reduced. Therefore, it could be simulated from the spectrum that the total amount of Cu^+, which were more active than Cu^{2+} during the reduction, increased from 19.67% to 40.78% after treatment. From the O 1s spectra (Figure S5), three different types of oxygen: absorbed O, vacancy O and Cu−O were observed, and the peak representing vacancy O increased after the treatment, which might be owing to the removal of the whole guest molecules and thus the missing oxygen. Additionally, Fourier transform infrared spectra (FT-IR) were collected to elucidate the chemical bonding features to learn more about the decomposition (Figure S7). A big wide peak ranging from 3000 to 3650 cm^{-1} was attributed from the hydrogen bonds of the hydroxyl groups.[34] The peaks appearing at 1366, 1448, and 1644 cm^{-1} were assigned to C−O stretching, C═O stretching, and the O−H bending vibrations of free carboxylic groups.[35] As we could see, these peaks were located at the same positions for Cu-MOF-74 and Cu-MOF-74-P_{60} catalysts, suggesting that the structure and organic bonding were maintained well after treatment. The intensity of the wide peak of the hydroxyl groups became weaken after the plasma treatment, illustrating the missing of some organic guests. It was in agreement with the result of XRD and XPS, also indicating the decomposition of the structure.

3.2. EPR Measurement and XAFS. The electron paramagnetic resonance (EPR) was carried out to research the ground state of the electron configuration in Cu-MOF-74 (Figure 2a, Figure S8). The unpaired electrons were directly influenced by the atomic coordination environment, the distance between atoms, and the oxidation state. With a longer time of Ar plasma treatment, the EPR signal intensity of Cu-MOF-74-P increased and the peak intensity became stronger compared with the as-prepared catalyst. Also, the g factor, which represents the total angular momentum of the unpaired electron, of Cu-MOF-74-P increased from 2.10 to 2.22 and then decreased to about 2.13 with longer treatment time (Figure S8). The sharpening EPR signal indicated increased unpaired electrons, which was related to the change of the atomic environment. From the XPS results, we could see that the Cu^{2+} was the main Cu species and the oxidation state of Cu got lower for Cu-MOF-74-P_{60} than Cu-MOF-74. Thus, the increase of the unpaired electron character in Cu-MOF-74-P could be interpreted by the change of the atomic distance and bonding strain.[25] A shoulder peak appearing at a magnetic field of 3200 G also demonstrated structural distortion, confirming the successful removal of partial organic ligands from the as-prepared materials. Therefore, the plasma process modulated the local atomic structure and the electron state of the active center.

To gain further insight into the structure changes and coordination environment changes of Cu-MOF-74 after plasma-engraving, X-ray absorption fine structure (XAFS) was carried out. The oxidation state, the bond distance, and the coordination number were clearly shown in X-ray absorption near edge structure (XANES) and extended X-ray absorption fine structure (EXAFS) pattern (Figure 2b). Moreover, a wavelet transform spectrum was obtained to present the EXAFS data through wavelet transforming of the χ(K), as shown in Figure 2d.

Interestingly, from the XANES, the K-edge of Cu-MOF-74 before and after treatment showed typical oxide characteristics at 8998 eV and were both located to the left of the standard CuO, indicating that their valence state was under the saturation state, which could account for their CO_2 reduction activity. Moreover, it could be seen that the K-edge of the Cu-MOF-74-P_{60} shifted toward a lower energy level compared to Cu-MOF-74, and the intensity of the white line peak also decreased accordingly. This proved that the valence state of Cu decreased partially to +1 after the treatment, which was consistent with the previous results obtained in the XPS analysis.[36] The catalyst had excellent reducibility, which might bring great reduction performance. From the R-space (k^3-weighted) spectrum of EXAFS, the main peak locating at the position of 1.52 Å was attributed to the Cu−O bond, indicating that Cu−O was the main coordination bond. The surrounding signal peaks might be some weak coordination structures or signal disturbances. Also after plasma engraving, the peak intensity of Cu-MOF-74-P_{60} significantly decreased, and it was found by fitting that the coordination number of Cu−O decreased from 2.7 to 1.6 (Table S1). Thus, the Cu got to a more unsaturated state, which also led to a decrease in the valence state of Cu. The wavelet transform spectrum further proved that Cu−O was the main coordination bond, and the strength of the central region decreased to about half, same as the fitting result.

Combining the above results, the amount of unpaired electrons in Cu-MOF-74-P_{60} increased after the plasma treatment. Confirming that part of the organic ligands in Cu-MOF-74 were removed, thus resulting in the decrease of the coordination number of Cu−O from 2.7 to 1.6. So this led to the oxidation state of Cu being partially reduced to +1. These results might promote the CO_2 activation and adsorption of *CO, thus improving the selectivity of the ERC.

3.3. ERC Activity Performance. The CO_2 electroreduction behavior experiment of Cu-MOF-74 was carried out in a flow cell (Figure S9) using 0.5 M $KHCO_3$ solution as electrolyte.[37,38] The cell was composed of a three-electrode system (physics), using a gas diffusion electrode (GDE) as the working electrode, a Ag/AgCl reference electrode, and a nickel foam mesh counter electrode. A piece of anion exchange membrane (3PK-130) was used to separate the cathode and the anode. And the FE for the production in the reduction was evaluated by nuclear magnetic resonance (NMR) and gas chromatography. Firstly, the effect of different intensities (80, 50, 40, 20, and 10 W) of the Ar plasma on the Cu-MOF-74 was investigated. Different powers with the same total energy output of the plasma were set. The FE distribution showed that the selectivity of C_2H_4 increased with the decrease of power while the product selectivity of CO showed a decreasing process and H_2 was also inhibited in this process with a decreasing trend (Figure S10), verifying the effect of coordination number modulation in promoting the C−C coupling of *CO to C_2 product and inhibiting the H_2 generation. Therefore, the best $FE_{C_2H_4}$ of about 25% was obtained at a power of 10 W, because more electrons strengthen the absorption of *CO and promote the C−C coupling. After setting the optimal plasma treating power as 10 W, the effect of different treating time on the catalyst was next explored. The Faradaic efficiency distribution of different products was displayed in Figures S11 and S12, showing that FE_{H_2} was suppressed to 10% on average. For Cu-MOF-74, the main product in ERC was CO with nearly 30% FE, while the C_2H_4 selectivity promoted from 15.1% to 25.1% in Cu-MOF-74-P_{40}, The $FE_{C_2H_4}$ increased to 48% for Cu-MOF-74-P_{60}, whose value was twice bigger than the original Cu-MOF-74

https://doi.org/10.1021/cbe.4c00021
Chem Bio Eng. 2024, 1, 836−845

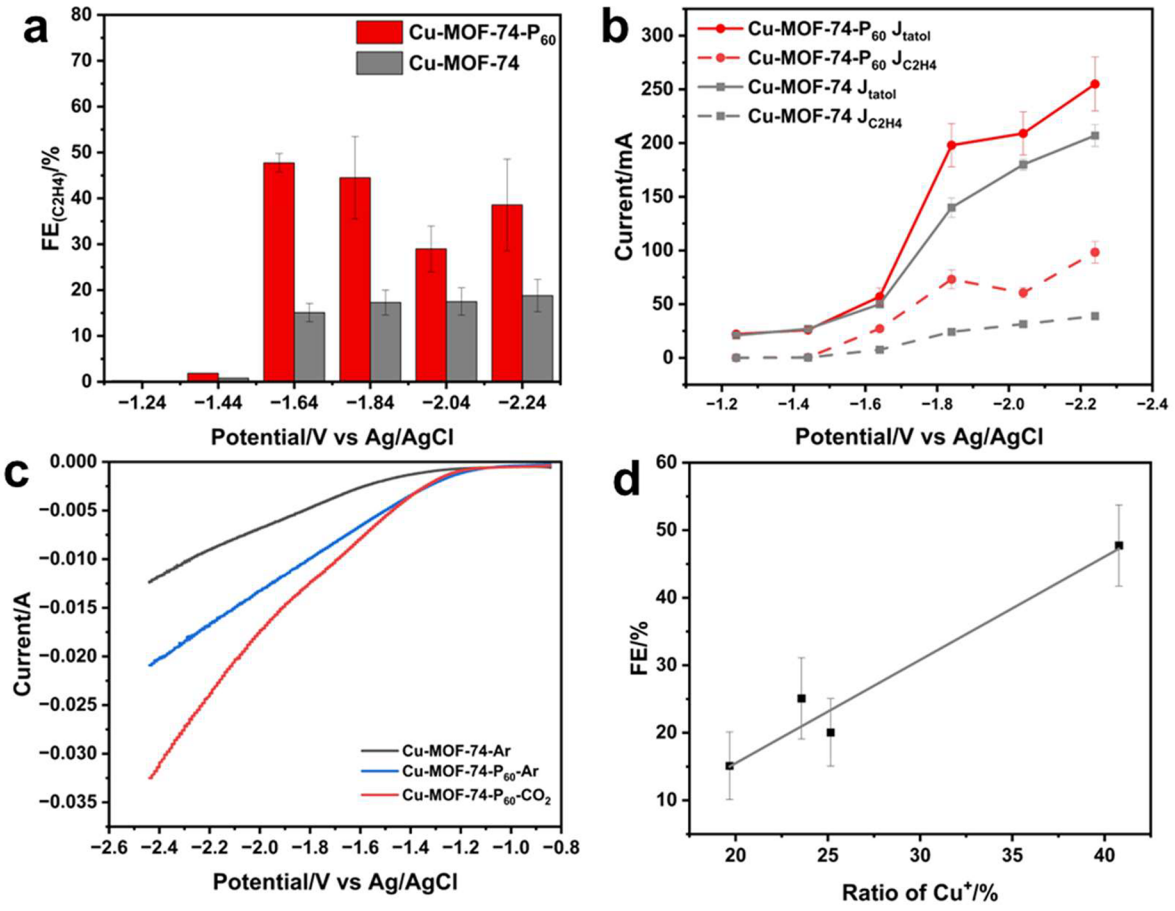

Figure 3. (a) Distribution of C_2H_4 for as-prepared Cu-MOF-74 and Cu-MOF-74-P_{60} under different potential. (b) Total and partial current of C_2H_4 of as-prepared Cu-MOF-74 and Cu-MOF-74-P_{60} under different potential. (c) Linear sweep voltammetry (LSV) carves of as-prepared Cu-MOF-74 in Ar gas, Cu-MOF-74-P_{60} in Ar gas and Cu-MOF-74-P_{60} in CO_2 gas. (d) Relationship between the $FE_{C_2H_4}$ and the ratio of the Cu^+ in Cu-MOF-74-P.

and was also higher than most $FE_{C_2H_4}$ reported for Cu-MOF based electrocatalyst up to date. Moreover, its FE_{CO} decreased to the minimum of 16.8%,[2,25,39] for being involved in the C−C coupling process to form ethylene products. This result indicated that the modulation had a great impact on promoting the reaction toward C_2 production and suppressing the H_2 production. Additionally, we could see that the total current of the four catalysts is nearly the same and around 60 mA/cm^2. But the Cu-MOF-74-P_{60} exhibited the largest partial density of C_2H_4, and there was a positive correlation between the partial current density of C_2H_4 and $FE_{C_2H_4}$ (Figure S13), suggesting that a bigger partial current density supports higher selectivity. Continuous electrolysis and product analysis under different voltages, measuring CO, H_2, C_2H_4, etc. at various voltages, were conducted on Cu-MOF-74-P_{60} (Figure S14). The $FE_{C_2H_4}$ could keep a high level near 40% among all potentials from −0.91 to −1.51 V vs reversible hydrogen electrode (RHE) (Figure 3a). As shown in Figure S14, H_2 was suppressed from 70% to 10%, with a slight increase at higher potential, which might be attributed to the enhanced HER due to an insufficient supply of CO_2 gas.[40] There was an interesting phenomenon that the C_2H_5OH formation was very high at lower potential while C_2H_4 formation was dominant at higher potential. It corresponds to the onset potential of C_2H_4 being higher than C_2H_5OH. So it could be summarized that the low potential was more in favor of generating liquid product while high potential favored the formation of gas product.[7,41,42] From Figure 3b, the total and partial current densities of the Cu-MOF-74-P_{60} were both bigger than those of Cu-MOF-74, along with better ERC performance. The current density increased with the applied potential shifting to more negative values, and the largest current density reached 255 mA/cm^2 at −1.51 V vs RHE.[43] Then, we analyzed changing the trend of $FE_{C_2H_4}$ and the ratio of the Cu^+ (Figure 3d), and the result showed that the larger ratio of Cu^+ was beneficial for the reduction process, matching well with the result of the ERC. What is more, we applied the Ar plasma on several other kinds of MOF (Cu-BTC, Cu-BDC, and Cu-AZA) catalysts and found that all of ERC behaviors had been improved on different degrees under different treatment time (Figures S15−S17). So, the plasma engraving is an effective strategy to regulate the ERC product selectivity. Furthermore, the optimal power for achieving the highest performance was different for every single MOF, which might be owing to the different bonding strength of the structure in different MOF. To investigate the stability of the catalyst under reaction conditions, it was found that after 120 min of continuous operation, the overall ethylene selectivity decreased by only 5% relative to the initial performance, while the current density remained nearly stable, and only a few 0-valent Cu was detected in the Cu LMM spectra of the catalysts after the

https://doi.org/10.1021/cbe.4c00021
Chem Bio Eng. 2024, 1, 836−845

reaction, as shown in the post-reaction Cu LMM characterizations. It could also be seen from the EPR diagram of the catalyst of post-reaction that the peak strength had not changed significantly (Figures S19 and S20). Hence, it could be seen that the structural stability was good.

To learn more about the electric behavior of the catalysts, the linear sweep voltammetry (LSV) was tested in a H-cell in both Ar- and CO_2-saturated 0.1 M $KHCO_3$ electrolyte.[38] As the result showed in Figure 3c, there were no peaks observed in this process, indicating no redox reaction on the catalyst.[44,45] Compared to as-prepared Cu-MOF-74 in Ar-saturated electrolyte, the Cu-MOF-74-P_{60} exhibited an earlier onset potential, and its current density was higher as well, indicating that the plasma treated catalyst processed a better electron transfer performance. Moreover, the Cu-MOF-74-P_{60} in CO_2-saturated reached a significantly larger current density than that in Ar-saturated, which directly illustrated that the plasma treatment boosted the ERC activity of Cu-MOF-74. The electrochemical active surface area (ECSA) is directly proportional to the double-layer capacitance (C_{dl}).[7] Therefore, the cyclic voltammetry (CV) experiment was carried out to calculate the C_{dl}. The double-layer capacitance results of the two catalysts in Figure S21 were nearly the same but the Cu-MOF-74-P_{60} had a larger active surface area.[45] Therefore, the better product selectivity and higher activity of the treated Cu-MOF-74-P could also be ascribed to larger active surface area. Then electrochemical impedance spectroscopy (EIS) was carried out over a frequency range from 0.1 to 10^5 Hz to study the charge transfer resistance of catalyst.[46] The plot in Figure S22 of Cu-MOF-74-P showed a smaller fitting semicircle compared to Cu-MOF-74 in the high-frequency region, suggesting that the Cu-MOF-74-P catalyst had smaller internal solution resistance and a faster charge transfer rate at the electrode/electrolyte interfaces. Hence, it could be concluded that the Ar plasma treatment also had an improvement in electron transfer performance to boost the ERC performance.

3.4. In Situ DRIFTS to Study Mechanism. To get further insight into the activity enhancement on Cu-MOF-74-P (here we compared Cu-MOF-74-P_{60} with Cu-MOF-74), in situ Fourier transform infrared spectroscopy (in situ DRIFTS) was conducted to monitor the intermediates occurred during the reduction with the potential ranging from 0 to −1 V vs RHE.[47] As Figure 4a,b showed, when the applied potential was below −0.4 V vs RHE, there was nearly no intermediate species existing. When the potential shifted to more negative, three peaks appeared at 2068−2035, 1820, and 1594 cm^{-1} respectively, attributed to the generated CO_{atop}, CO_{bridge}, and *COOH bound to the catalyst surface.[48−50] The peaks from 1600 to 1500 cm^{-1} were assigned to the signal of HCO_3^-. The red shift in the vibrational frequency of CO_{atop} was ascribed to the vibrational stark effect of CO_{atop} molecules or electron back-donation from the Cu surface to the *CO_{atop} molecules.[51] The *COOH intermediates could then transform into *CO, and *CO was the key species to generate C_2 product through C−C coupling. As we could see the FT-IR pattern of as-prepared Cu-MOF-74, the intensity of the CO_{atop} formed on the Cu surface throughout the CO_2 reduction was lower than that of Cu-MOF-74-P_{60}, which could explain the higher selectivity and activity of C_2 production on the Cu-MOF-74-P_{60}. The *CO_{bridge} was observed at 1820 cm^{-1} from −0.4 V vs RHE to the end in Cu-MOF-74-P_{60}, which only appeared at −0.4 V vs RHE and soon disappeared in the as-prepared Cu-MOF-74. The intensity of the *CO_{bridge} peak represented the abundant coverage of *CO. The more coverage of both *CO_{atop} and *CO_{bridge} promoted the C−C coupling, which was consistent with higher C_2H_4 formation on the Cu-MOF-74-P_{60}. Also the *COOH intermediate that appeared on Cu-MOF-74-P_{60} during the potential scanning was beneficial to improve the coverage of *CO so as to further promote the C−C coupling and C_2 production.[52] These evidences confirmed that *CO_{atop} and CO_{bridge} were the important intermediates for the formation of C_2H_4, and the sufficient *CO on Cu-MOF-74-P_{60} promoted higher selectivity of C_2H_4.

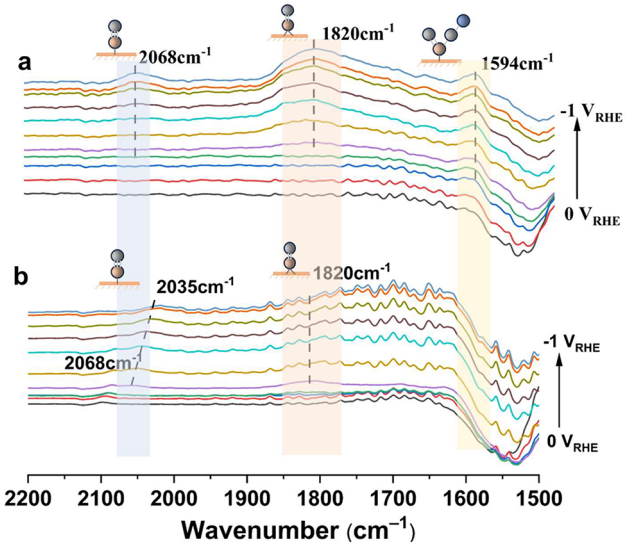

Figure 4. (a) (b) In situ Fourier transform infrared spectroscopy of as-prepared Cu-MOF-74 and Cu-MOF-74-P_{60} under the potentials ranging from 0 to −1.0 V (vs RHE) at an interval of 0.1 V.

To summarize, through the plasma treatment, part of the organic ligands in Cu-MOF-74 were removed, thus resulting in the decrease of Cu−O coordination number. Thus, the density of the unpaired electrons would increase, which will promote the activation of CO_2 and adsorption of the *CO. So the coverage of *CO would also increase to facilitate the C−C coupling. Meanwhile, the amount of Cu^+ after room-temperature plasma-engraving had largely increased and thus the energy barrier got lower than on Cu^{2+}, which would also improve the C−C coupling and C_2 production selectivity. With in situ DRIFTS, it was further found that the improvement of the ECR activity was closely related to the coverage of the CO_{atop} and CO_{bridge} intermediates bound to the Cu-MOF-74 surface.

4. CONCLUSIONS

In summary, this work proposed a simple but effective strategy to modulate the coordination environment of Cu sites in the ERC for selective electroreduction of CO_2 to C_2H_4. The room-temperature plasma treatment was conducted to remove part of the organic ligands for increasing the unsaturated Cu catalytic sites. It was found that the overall framework structure of the MOF could be maintained and the spatial structure was adjusted during the treatment with different powers of plasma. Imposing lower intensity plasma and longer time was more beneficial to improve the catalyst activity, achieving a significant increase in the selectivity of C_2H_4 to 48% during the ERC. The results of in situ DRIFTS and XAFS showed that the room-temperature plasma treatment process increased

https://doi.org/10.1021/cbe.4c00021
Chem Bio Eng. 2024, 1, 836−845

the unsaturation of the Cu active site. Therefore, the amount of the absorbed *CO intermediates increased during the reaction, and the C−C coupling was strengthened to achieve higher selectivity of C_2H_4.

■ ASSOCIATED CONTENT

Supporting Information

The Supporting Information is available free of charge at https://pubs.acs.org/doi/10.1021/cbe.4c00021.

Experimental detail; SEM, TEM, and EDS images of electrocatalysts; Cu 2p, O 1s, and Cu LMM XPS spectra of electrocatalysts; FTIR spectra of electrocatalysts; EPR and XPS spectra; schematic diagram of flow cell; FEs of different powers, treating times, and potentials; total current and partial current; C_2H_4 selectivity of different MOFs; stability of electrocatalysts; CVs and C_{dl} of electrocatalysts; Nyquist plots; XAFS fitting parameters (PDF)

■ AUTHOR INFORMATION

Corresponding Authors

Yao Shen − *Key Laboratory of Microbial Technology for Industrial Pollution Control of Zhejiang Province, College of Environment, Zhejiang University of Technology, Hangzhou 310014, China*; Email: yaoshen@zjut.edu.cn

Sujing Li − *Key Laboratory of Biomass Chemical Engineering of the Ministry of Education, Institute of Industrial Ecology and Environment, College of Chemical and Biological Engineering, Zhejiang University, Hangzhou 310027, China*; orcid.org/0000-0002-7757-3881; Email: sujing-li@zju.edu.cn

Authors

Wenfu Luo − *Key Laboratory of Biomass Chemical Engineering of the Ministry of Education, Institute of Industrial Ecology and Environment, College of Chemical and Biological Engineering, Zhejiang University, Hangzhou 310027, China*

Shijie Li − *Key Laboratory of Biomass Chemical Engineering of the Ministry of Education, Institute of Industrial Ecology and Environment, College of Chemical and Biological Engineering, Zhejiang University, Hangzhou 310027, China*

Shihan Zhang − *Key Laboratory of Microbial Technology for Industrial Pollution Control of Zhejiang Province, College of Environment, Zhejiang University of Technology, Hangzhou 310014, China*; orcid.org/0000-0002-2377-5760

Wei Li − *Key Laboratory of Biomass Chemical Engineering of the Ministry of Education, Institute of Industrial Ecology and Environment, College of Chemical and Biological Engineering, Zhejiang University, Hangzhou 310027, China*; orcid.org/0000-0002-6216-9499

Complete contact information is available at: https://pubs.acs.org/10.1021/cbe.4c00021

Notes

The authors declare no competing financial interest.

■ ACKNOWLEDGMENTS

The authors acknowledge the financial support from "Pioneer" and "Leading Goose" R&D Program of Zhejiang (No. 2023C03017 and No. 2022C03146) and National Funded Postdoctoral Researcher Program of China (No. GZC20232363).

■ REFERENCES

(1) Duan, Y. X.; Zhou, Y. T.; Yu, Z.; Liu, D. X.; Wen, Z.; Yan, J. M.; Jiang, Q. Boosting Production of HCOOH from CO_2 Electroreduction via Bi/CeO_x. *Angew. Chem., Int. Ed.* **2021**, *60*, 8798−8802.

(2) Xie, M. S.; Xia, B. Y.; Li, Y.; Yan, Y.; Yang, Y.; Sun, Q.; Chan, S. H.; Fisher, A.; Wang, X. Amino acid modified copper electrodes for the enhanced selective electroreduction of carbon dioxide towards hydrocarbons. *Energy Environ. Sci.* **2016**, *9*, 1687−1695.

(3) Verma, S.; Lu, S.; Kenis, P. J. A. Co-electrolysis of CO_2 and glycerol as a pathway to carbon chemicals with improved technoeconomics due to low electricity consumption. *Nat. Energy* **2019**, *4*, 466−474.

(4) Liu, A.; Gao, M.; Ren, X.; Meng, F.; Yang, Y.; Gao, L.; Yang, Q.; Ma, T. Current progress in electrocatalytic carbon dioxide reduction to fuels on heterogeneous catalysts. *J. Mater. Chem. A* **2020**, *8*, 3541−3562.

(5) Yi, J. D.; Si, D. H.; Xie, R.; Yin, Q.; Zhang, M. D.; Wu, Q.; Chai, G. L.; Huang, Y. B.; Cao, R. Conductive Two-Dimensional Phthalocyanine-based Metal-Organic Framework Nanosheets for Efficient Electroreduction of CO_2. *Angew. Chem., Int. Ed.* **2021**, *60*, 17108−17114.

(6) Zhang, J.; Yin, R.; Shao, Q.; Zhu, T.; Huang, X. Oxygen Vacancies in Amorphous InO_x Nanoribbons Enhance CO_2 Adsorption and Activation for CO_2 Electroreduction. *Angew. Chem., Int. Ed.* **2019**, *58*, 5609−5613.

(7) Chen, Q.; Wang, X.; Zhou, Y.; Tan, Y.; Li, H.; Fu, J.; Liu, M. Electrocatalytic CO_2 Reduction to C_{2+} Products in Flow Cells. *Adv. Mater.* **2024**, *36*, No. e2303902.

(8) Wang, Y.; Liu, J.; Zheng, G. Designing Copper-Based Catalysts for Efficient Carbon Dioxide Electroreduction. *Adv. Mater.* **2021**, *33*, No. e2005798.

(9) Yin, J.; Gao, Z.; Wei, F.; Liu, C.; Gong, J.; Li, J.; Li, W.; Xiao, L.; Wang, G.; Lu, J.; Zhuang, L. Customizable CO_2 Electroreduction to C_1 or C_{2+} Products through Cuy/CeO_2 Interface Engineering. *ACS Catal.* **2022**, *12*, 1004−1011.

(10) Ren, X.; Zhang, X.; Cao, X.; Wang, Q. Efficient electrochemical reduction of carbon dioxide into ethylene boosted by copper vacancies on stepped cuprous oxide. *J. CO_2 Util.* **2020**, *38*, 125−131.

(11) Wang, J.; Zheng, X.; Wang, G.; Cao, Y.; Ding, W.; Zhang, J.; Wu, H.; Ding, J.; Hu, H.; Han, X.; Ma, T.; Deng, Y.; Hu, W. Defective Bimetallic Selenides for Selective CO_2 Electroreduction to CO. *Adv. Mater.* **2022**, *34*, No. e2106354.

(12) Xiao, H.; Goddard, W. A.; Cheng, T.; Liu, Y. Cu metal embedded in oxidized matrix catalyst to promote CO_2 activation and CO dimerization for electrochemical reduction of CO_2. *Proc. Natl. Acad. Sci. U.S.A.* **2017**, *114*, 6685−6688.

(13) Gong, Y. N.; Cao, C. Y.; Shi, W. J.; Zhang, J. H.; Deng, J. H.; Lu, T. B.; Zhong, D. C. Modulating the Electronic Structures of Dual-Atom Catalysts via Coordination Environment Engineering for Boosting CO_2 Electroreduction. *Angew. Chem., Int. Ed.* **2022**, *61*, No. e202215187.

(14) Wang, Y.; Liu, Y.; Liu, W.; Wu, J.; Li, Q.; Feng, Q.; Chen, Z.; Xiong, X.; Wang, D.; Lei, Y. Regulating the coordination structure of metal single atoms for efficient electrocatalytic CO_2 reduction. *Energy Environ. Sci.* **2020**, *13*, 4609−4624.

(15) Zhang, Y.; Jiao, L.; Yang, W.; Xie, C.; Jiang, H. L. Rational Fabrication of Low-Coordinate Single-Atom Ni Electrocatalysts by MOFs for Highly Selective CO_2 Reduction. *Angew. Chem., Int. Ed.* **2021**, *60*, 7607−7611.

(16) Hou, X.; Ding, J.; Liu, W.; Zhang, S.; Luo, J.; Liu, X. Asymmetric Coordination Environment Engineering of Atomic Catalysts for CO_2 Reduction. *Nanomaterials (Basel)* **2023**, *13*, 309.

(17) Qiu, L.; Shen, S.; Ma, C.; Lv, C.; Guo, X.; Jiang, H.; Liu, Z.; Qiao, W.; Ling, L.; Wang, J. Controllable fabrication of atomic dispersed low-coordination nickel-nitrogen sites for highly efficient electrocatalytic CO_2 reduction. *Chem. Eng. J.* **2022**, *440*, 135956.

(18) Zhu, W.; Zhang, L.; Yang, P.; Hu, C.; Luo, Z.; Chang, X.; Zhao, Z. J.; Gong, J. Low-Coordinated Edge Sites on Ultrathin Palladium Nanosheets Boost Carbon Dioxide Electroreduction Performance. *Angew. Chem., Int. Ed.* **2018**, *57*, 11544−11548.
(19) Su, P.; Iwase, K.; Harada, T.; Kamiya, K.; Nakanishi, S. Covalent triazine framework modified with coordinatively-unsaturated Co or Ni atoms for CO_2 electrochemical reduction. *Chem. Sci.* **2018**, *9*, 3941−3947.
(20) Li, Y.; Karimi, M.; Gong, Y.-N.; Dai, N.; Safarifard, V.; Jiang, H.-L. Integration of metal-organic frameworks and covalent organic frameworks: Design, synthesis, and applications. *Matter* **2021**, *4*, 2230−2265.
(21) Diercks, C. S.; Liu, Y.; Cordova, K. E.; Yaghi, O. M. The role of reticular chemistry in the design of CO_2 reduction catalysts. *Nat. Mater.* **2018**, *17*, 301−307.
(22) Hao, L.; Xia, Q.; Zhang, Q.; Masa, J.; Sun, Z. Improving the performance of metal-organic frameworks for thermo-catalytic CO_2 conversion: Strategies and perspectives. *Chin. J. Catal.* **2021**, *42*, 1903−1920.
(23) Zhou, D.; Li, X.; Shang, H.; Qin, F.; Chen, W. Atomic regulation of metal-organic framework derived carbon-based single-atom catalysts for the electrochemical CO_2 reduction reaction. *J. Mater. Chem. A* **2021**, *9*, 23382−23418.
(24) Wei, S.; Jiang, X.; He, C.; Wang, S.; Hu, Q.; Chai, X.; Ren, X.; Yang, H.; He, C. Construction of single-atom copper sites with low coordination number for efficient CO_2 electroreduction to CH_4. *J. Mater. Chem. A* **2022**, *10*, 6187−6192.
(25) Nam, D. H.; Bushuyev, O. S.; Li, J.; De Luna, P.; Seifitokaldani, A.; Dinh, C. T.; Garcia de Arquer, F. P.; Wang, Y.; Liang, Z.; Proppe, A. H.; Tan, C. S.; Todorovic, P.; Shekhah, O.; Gabardo, C. M.; Jo, J. W.; Choi, J.; Choi, M. J.; Baek, S. W.; Kim, J.; Sinton, D.; Kelley, S. O.; Eddaoudi, M.; Sargent, E. H. Metal-Organic Frameworks Mediate Cu Coordination for Selective CO_2 Electroreduction. *J. Am. Chem. Soc.* **2018**, *140*, 11378−11386.
(26) Von Keudell, A.; Schulz-von der Gathen, V. Foundations of low-temperature plasma physics—an introduction. *Plasma Sources Sci. Technol.* **2017**, *26*, 113001.
(27) Stauss, S.; Muneoka, H.; Terashima, K. Review on plasmas in extraordinary media: plasmas in cryogenic conditions and plasmas in supercritical fluids. *Plasma Sources Sci. Technol.* **2018**, *27*, 023003.
(28) Song, J.; Zhao, S.; Liu, D.; Xiong, Y.; Hu, F.; Li, L.; Li, L.; Pan, H.; Peng, S. Plasma-induced defect engineering of porous metal-organic framework nanosheet arrays for efficient water splitting. *Chem. Commun. (Cambridge, U. K.)* **2022**, *58*, 9662−9665.
(29) Leo, P.; Orcajo, G.; Briones, D.; Calleja, G.; Sanchez-Sanchez, M.; Martinez, F. A Recyclable Cu-MOF-74 Catalyst for the Ligand-Free O-Arylation Reaction of 4-Nitrobenzaldehyde and Phenol. *Nanomaterials (Basel)* **2017**, *7*, 149.
(30) Zheng, H.; Wang, D.; Sun, X.; Jiang, S.; Liu, Y.; Zhang, D.; Zhang, L. Surface modified by green synthetic of Cu-MOF-74 to improve the anti-biofouling properties of PVDF membranes. *Chem. Eng. J.* **2021**, *411*, 128524.
(31) Zheng, H.; Zhou, Y.; Wang, D.; Zhu, M.; Sun, X.; Jiang, S.; Fan, Y.; Zhang, D.; Zhang, L. Surface-functionalized PVDF membranes by facile synthetic Cu-MOF-74 for enhanced contaminant degradation and antifouling performance. *Colloids Surf., A* **2022**, *651*, 129640.
(32) Todaro, M.; Buscarino, G.; Sciortino, L.; Alessi, A.; Messina, F.; Taddei, M.; Ranocchiari, M.; Cannas, M.; Gelardi, F. M. Decomposition Process of Carboxylate MOF HKUST-1 Unveiled at the Atomic Scale Level. *J. Phys. Chem. C* **2016**, *120*, 12879−12889.
(33) Yao, K.; Xia, Y.; Li, J.; Wang, N.; Han, J.; Gao, C.; Han, M.; Shen, G.; Liu, Y.; Seifitokaldani, A.; Sun, X.; Liang, H. Metal-organic framework derived copper catalysts for CO_2 to ethylene conversion. *J. Mater. Chem. A* **2020**, *8*, 11117−11123.
(34) Shi, Y.-N.; Zhang, F.; Chan, K. L.; Li, W.; Lin, H.; Duan, M. An improved Eddington approximation method for irradiance calculation in a vertical inhomogeneous medium. *J. Quant. Spectrosc. Radiat. Transfer* **2019**, *226*, 40−50.
(35) Jun, B. M.; Kim, S.; Kim, Y.; Her, N.; Heo, J.; Han, J.; Jang, M.; Park, C. M.; Yoon, Y. Comprehensive evaluation on removal of lead by graphene oxide and metal organic framework. *Chemosphere* **2019**, *231*, 82−92.
(36) Jia, J.; Zhao, X.; Hu, W.; Wang, Y.; Huang, J.; Huang, J.; Li, H.; Peng, Y.; Ma, H.; Xu, C. Role of cobalt phthalocyanine on the formation of high-valent cobalt species revealed by in situ Raman spectroscopy. *J. Mater. Chem. A* **2023**, *11*, 8141−8149.
(37) Ji, L.; Chang, L.; Zhang, Y.; Mou, S.; Wang, T.; Luo, Y.; Wang, Z.; Sun, X. Electrocatalytic CO_2 Reduction to Alcohols with High Selectivity over a Two-Dimensional $Fe_2P_2S_6$ Nanosheet. *ACS Catal.* **2019**, *9*, 9721−9725.
(38) Ye, L.; Ying, Y.; Sun, D.; Zhang, Z.; Fei, L.; Wen, Z.; Qiao, J.; Huang, H. Highly Efficient Porous Carbon Electrocatalyst with Controllable N-Species Content for Selective CO_2 Reduction. *Angew. Chem., Int. Ed.* **2020**, *59*, 3244−3251.
(39) Sun, Y.; Xie, J.; Fu, Z.; Zhang, H.; Yao, Y.; Zhou, Y.; Wang, X.; Wang, S.; Gao, X.; Tang, Z.; Li, S.; Wang, X.; Nie, K.; Yang, Z.; Yan, Y. M. Boosting CO_2 Electroreduction to C_2H_4 via Unconventional Hybridization: High-Order Ce^{4+} 4f and O 2p Interaction in Ce-Cu_2O for Stabilizing Cu^+. *ACS Nano* **2023**, *17*, 13974−13984.
(40) Wei, Z.; Ding, J.; Duan, X.; Chen, G.-L.; Wu, F.-Y.; Zhang, L.; Yang, X.; Zhang, Q.; He, Q.; Chen, Z.; Huang, J.; Hung, S.-F.; Yang, X.; Zhai, Y. Enhancing Selective Electrochemical CO_2 Reduction by In Situ Constructing Tensile-Strained Cu Catalysts. *ACS Catal.* **2023**, *13*, 4711−4718.
(41) Liu, M.; Wang, Q.; Luo, T.; Herran, M.; Cao, X.; Liao, W.; Zhu, L.; Li, H.; Stefancu, A.; Lu, Y.-R.; Chan, T.-S.; Pensa, E.; Ma, C.; Zhang, S.; Xiao, R.; Cortés, E. Potential Alignment in Tandem Catalysts Enhances CO_2-to-C_2H_4 Conversion Efficiencies. *J. Am. Chem. Soc.* **2024**, *146*, 468−475.
(42) Zi, X.; Zhou, Y.; Zhu, L.; Chen, Q.; Tan, Y.; Wang, X.; Sayed, M.; Pensa, E.; Geioushy, R. A.; Liu, K.; Fu, J.; Cortés, E.; Liu, M. Breaking K^+ Concentration Limit on Cu Nanoneedles for Acidic Electrocatalytic CO_2 Reduction to Multi-Carbon Products. *Angew. Chem., Int. Ed.* **2023**, *62*, No. e202309351.
(43) Zhang, J.; Li, Z.; Xia, S.; Zhang, T.; Wang, Y.; Wu, Y.; Wu, J. Reconstructing two-dimensional defects in CuO nanowires for efficient CO_2 electroreduction to ethylene. *Chem. Commun. (Cambridge, U. K.)* **2021**, *57*, 8276−8279.
(44) Yi, J. D.; Xie, R.; Xie, Z. L.; Chai, G. L.; Liu, T. F.; Chen, R. P.; Huang, Y. B.; Cao, R. Highly Selective CO_2 Electroreduction to CH_4 by In Situ Generated Cu_2O Single-Type Sites on a Conductive MOF: Stabilizing Key Intermediates with Hydrogen Bonding. *Angew. Chem., Int. Ed.* **2020**, *59*, 23641−23648.
(45) Liu, S.; Xiao, J.; Lu, X. F.; Wang, J.; Wang, X.; Lou, X. W. D. Efficient Electrochemical Reduction of CO_2 to HCOOH over Sub-2 nm SnO_2 Quantum Wires with Exposed Grain Boundaries. *Angew. Chem., Int. Ed.* **2019**, *58*, 8499−8503.
(46) Giusi, D.; Miceli, M.; Genovese, C.; Centi, G.; Perathoner, S.; Ampelli, C. In situ electrochemical characterization of CuxO-based gas-diffusion electrodes (GDEs) for CO_2 electrocatalytic reduction in presence and absence of liquid electrolyte and relationship with C_{2+} products formation. *Appl. Catal., B* **2022**, *318*, 121845.
(47) Yan, C.; Luo, W.; Yuan, H.; Liu, G.; Hao, R.; Qin, N.; Wang, Z.; Liu, K.; Wang, Z.; Cui, D.; Hu, Z.; Lan, Y.; Lu, Z. Stabilizing intermediates and optimizing reaction processes with N doping in Cu_2O for enhanced CO_2 electroreduction. *Appl. Catal., B* **2022**, *308*, 121191.
(48) Wang, Y. R.; Ding, H. M.; Ma, X. Y.; Liu, M.; Yang, Y. L.; Chen, Y.; Li, S. L.; Lan, Y. Q. Imparting CO_2 Electroreduction Auxiliary for Integrated Morphology Tuning and Performance Boosting in a Porphyrin-based Covalent Organic Framework. *Angew. Chem., Int. Ed.* **2022**, *61*, No. e202114648.
(49) Jiang, T.-W.; Zhou, Y.-W.; Ma, X.-Y.; Qin, X.; Li, H.; Ding, C.; Jiang, B.; Jiang, K.; Cai, W.-B. Spectrometric Study of Electrochemical CO_2 Reduction on Pd and Pd-B Electrodes. *ACS Catal.* **2021**, *11*, 840−848.

https://doi.org/10.1021/cbe.4c00021
Chem Bio Eng. 2024, 1, 836−845

(50) Papasizza, M.; Cuesta, A. In Situ Monitoring Using ATR-SEIRAS of the Electrocatalytic Reduction of CO_2 on Au in an Ionic Liquid/Water Mixture. *ACS Catal.* **2018**, *8*, 6345−6352.
(51) Yau, S. L.; Gao, X.; Chang, S. C.; Schardt, B. C.; Weaver, M. J. Atomic-Resolution Scanning Tunneling Microscopy andInfrared Spectroscopy as Combined in Situ Probes of Electrochemical Adlayer Structure::Carbon Monoxide on Rhodium(111). *J. Am. Chem. Soc.* **1991**, *113*, 6049−6056.
(52) Gao, D.; Zhang, Y.; Zhou, Z.; Cai, F.; Zhao, X.; Huang, W.; Li, Y.; Zhu, J.; Liu, P.; Yang, F.; Wang, G.; Bao, X. Enhancing CO_2 Electroreduction with the Metal-Oxide Interface. *J. Am. Chem. Soc.* **2017**, *139*, 5652−5655.

https://doi.org/10.1021/cbe.4c00021
Chem Bio Eng. 2024, 1, 836−845